10	Li Y, Nagira T, Tsuchiya T	The effect of hyaluronic acid on insulin secretion in HIT-T15 cells through the enhancement of gap-junctional intercellular communications	Biomaterials	27 (8)	1437-1443	2006
11	Li YP, Nagira T, Tsuchiya T	Increase in the insulin secretion of HIT-T15 cells: Gap Junctional Intercellular Communications Enhanced by Hyaluronic Acid	Animal Cell Technology	14	263-269	2006
12	Nakamura N, Tsuchiya T	Effect of biodegradable polymer poly(L-LACTIC ACID) on the cellular function of human astrocytes	Animal Cell Technology	14	331-337	2006
13	Nakaoka R, Hsiong S, DJ. M	Regulation of chodrocyte differentiation via co-culture with osteoblasts	Tissue Engineering	12 (9)	2425-2433	2006
14	Nakaoka R, Tsuchiya T	Enhancement of Differentiation and Homeostasis of Human Osteoblasts by Interaction with Hydroxyapatite in Microsphere Form	Key Engineering Materials	309-31 (2)	1293-1296	2006
15	Sawada R, Ito T, Matsuda Y, Tsuchiya T	Safety evaluation of tissue engineered medical devices using normal human mesenchymal stem cells	Animal Cell Technology	14	325-329	2006
16	Sawada R, Ito T, Tsuchiya T	Changes in expression of genes related to cell population in human mesenchymal stem cells during in vitro culture in comparison with cancer cells	J. Artificial Organs	9	179-184	2006
17	Tamai M, Nakaoka R, Isama K, Tsuchiya T	Novel Calcium Phosphate Ceramics: The Remarkable Promoting Action on the Differentiation of the Normal Human Osteoblasts	Key Engineering Materials	309-311 (1)	97-100	2006
18	Tamai M, Nakaoka R, Tsuchiya T	Cytotoxicity of Various Calcium Phosphate Ceramics	Key Engineering Materials	309-311 (1)	263-266	2006
19	米山隆之, 川端隆司, 岡野光夫, 明石満, 土屋利江, 堤定美, 松下富春	バイオマテリアルと未来社会	バイオマテリアルー生体材料	24(1)	11-24	2006

19

Preparation of Protein Crystals for X-Ray Structural Study

Soichi Takeda

Summary

The knowledge of accurate molecular structures obtained by X-ray protein crystallography is now inevitable for rational drug design and for understanding the molecular basis underlying genetic disorders found in patients. However, preparing protein crystals suitable for structural analysis is currently the bottleneck in structure determination by this method. The intent of this chapter is to present current methods of preparing protein crystals for structural studies for a wide range of biologists who have access to macromolecules but do not know how to handle them for crystallization. The chapter includes the pretreatment of a protein prior to the crystallization experiment, initial screens, and optimization of the crystallization conditions for further X-ray study. Finally, handling considerations that are important for a protein intended for crystallization experiments are discussed.

Key Words: X-ray crystallography; structural biology; crystallization; protein structure; rational drug design; synchrotron.

1. Introduction

The importance of solving protein structures continues to grow in fields ranging from basic biochemistry and biophysics to pharmaceutical development, medical science, and, of course, cardiovascular research. In order to obtain high-resolution, three-dimensional structural knowledge of proteins by X-ray crystallography, crystals diffracting at high resolution are needed. This chapter focuses on the essential principles and procedures involved in crystallization so as to provide a general understanding of what is entailed in this key step of solving X-ray protein structures. It is not our aim to convert biologists into X-ray crystallographers; complete explanation of the physical basis of the techniques and methods currently practiced is beyond the scope of this chapter.

From: *Methods in Molecular Medicine, vol. 129: Cardiovascular Disease: Methods and Protocols, Volume 2: Molecular Medicine*
Edited by: Q. K. Wang © Humana Press Inc., Totowa, NJ

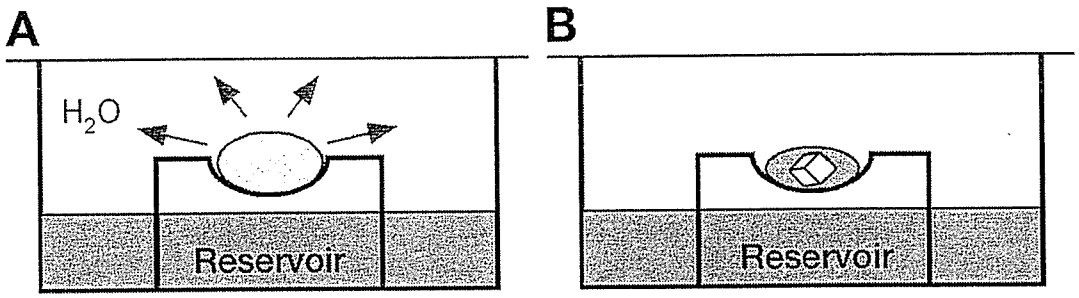

Fig. 1. Principle of the vapor diffusion (sitting drop) method for crystallization. The concentration of the reservoir is initially twice that in the droplet **(A)**, and the two become equal to that of the reservoir that has a volume several orders of magnitude larger than the droplet. The drop decreases volume during the process so that the concentration of all components in the drop, including the protein, rise significantly. If the variables are right, this results in protein crystallization **(B)**.

This chapter includes neither protein expression and purification protocols nor methods associated with X-ray diffraction data collection and structural analysis; rather, it simply focuses on the basis of crystallization experiments. If one needs further information as well as more detailed protocols on crystallization, please see the textbooks listed in the references *(1–7)*.

Although there are a variety of methods for setting up protein samples for crystallization, the most widely used method is crystallization by vapor diffusion. In this method, vapor diffusion occurs in a closed system because of a difference in concentration between a small droplet of protein, typically 0.3–10 μL, and a larger body of liquid, typically 0.1–1 mL (*see* **Fig. 1**). The protein drop is made by diluting protein twofold with liquid from the larger body, usually referred as the reservoir solution; therefore, the protein drop starts at half the concentration of the contents in the reservoir solution. This concentration gradient drives vapor diffusion, resulting in the gradual concentration of protein and, if the variables are right, protein crystallization. Reservoir solutions can contain a wide range of chemical variables, including buffers for pH control, salts (NaCl, ammonium sulfate, and so on), precipitating agents (polyethylene glycol, organic solvents), reducing agents (dithiothreitol and so on), and detergents.

As the variability of conditions required for crystallizing proteins is too large for exhaustive searches, more practical approaches for initial searches are employed. This is termed "sparse matrix" screening. The sparse matrix design was first introduced in 1991 by Jancarik and Kim *(8)* (*see* **Table 1** and **Note 1**). Various ready-made kits, some are the extensions of the original one and the others are based on different strategies, are currently commercially available and are used effectively for initial crystallization screens of large numbers of proteins.

Table 1
Fifty Solutions for the Original Sparse Matrix Screen *(7)*

No.	Salt	Buffer	Precipitant
1	0.02 *M* Ca chloride	0.1 *M* Na acetate pH 4.6	30% MPD
2	None	None	0.4 *M* K/Na Tartrate
3	None	None	0.4 *M* ammonium phosphate
4	None	0.1 *M* Tris-HCl pH 8.5	2.0 *M* ammonium sulfate
5	0.2 *M* Na citrate	0.1 *M* HEPES/NaOH pH 7.5	30% MPD
6	0.2 *M* Mg chloride	0.1 *M* Tris/HCl pH 8.5	30% PEG4000
7	None	0.1 *M* Na cacodylate pH 6.5	1.4 *M* Na acetate
8	0.2 *M* Na citrate	0.1 *M* Na cacodylate pH 6.5	30% iso-propanol
9	0.2 *M* ammonium acetate	0.1 *M* Na citrate pH 5.6	30% PEG 4000
10	0.2 *M* ammonium acetate	0.1 *M* Na acetate pH 4.6	30% PEG 4000
11	None	0.1 *M* Na citrate pH 5.6	1.0 *M* ammonium phosphate
12	0.2 *M* Mg chloride	0.1 *M* HEPES-Na pH 7.5	30% iso-propanol
13	0.2 *M* Na citrate	0.1 *M* Tris-HCl pH 8.5	30% PEG 400
14	0.2 *M* Ca chloride	0.1 *M* HEPES/NaOH pH 7.5	28% PEG 400
15	0.2 *M* ammonium sulfate	0.1 *M* Na cacodylate pH 6.5	30% PEG 8000
16	None	0.1 *M* HEPES/NaOH pH 7.5	1.5 *M* Li sulfate
17	0.2 *M* Li sulfate	0.1 *M* Tris/HCl pH 8.5	30% PEG 4000
18	0.2 *M* Mg acetate	0.1 *M* Na cacodylate pH 6.5	20% PEG 8000
19	0.2 *M* ammonium acetate	0.1 *M* Tris-HCl pH 8.5	30% iso-propanol
20	0.2 *M* ammonium sulfate	0.1 *M* Na acetate pH 4.6	25% PEG 4000
21	0.2 *M* Mg acetate	0.1 *M* Na cacodylate pH 6.5	30% MPD
22	0.2 *M* Na acetate	0.1 *M* Tris-HCl pH 8.5	30% PEG 4000
23	0.2 *M* Mg chloride	0.1 *M* HEPES/NaOH pH 7.5	30% PEG 400
24	0.2 *M* Ca chloride	0.1 *M* Na acetate pH 4.6	20% iso-propanol
25	None	0.1 *M* imidazole pH 6.5	1.0 *M* Na acetate
26	0.2 *M* ammonium acetate	0.1 *M* Na citrate pH 5.6	30% MPD
27	0.2 *M* Na citrate	0.1 *M* HEPES/NaOH pH 7.5	20% iso-propanol
28	0.2 *M* Na acetate	0.1 *M* Na cacodylate pH 6.5	30% PEG 8000
29	None	0.1 *M* HEPES/NaOH 7.5	0.8 *M* K/Na tartrate

(Continued)

Table 1 *(Continued)*
Fifty Solutions for the Original Sparse Matrix Screen *(7)*

No.	Salt	Buffer	Precipitant
30	0.2 *M* ammonium sulfate	None	30% PEG 8000
31	0.2 *M* ammonium sulfate	None	30% PEG 4000
32	None	None	2.0 *M* ammonium sulfate
33	None	None	4.0 *M* Na formate
34	None	0.1 *M* Na acetate pH 4.6	2.0 *M* Na formate
35	None	0.1 *M* HEPES/NaOH 7.5	0.8 *M* Na/K phosphate
36	None	0.1 *M* Tris-HCl pH 8.5	8% PEG 8000
37	None	0.1 *M* Na acetate pH 4.6	8% PEG 4000
38	None	0.1 *M* HEPES/NaOH pH 7.5	1.4 *M* Na citrate
39	2.0 *M* ammonium sulfate	0.1 *M* HEPES/NaOH pH 7.5	2% PEG 400
40	None	0.1 *M* Na citrate pH 5.6	20% iso-propanol, 20% PEG 4000
41	None	0.1 *M* HEPES/NaOH pH 7.5	10% iso-propanol, 20% PEG 4000
42	0.05 *M* K phosphate	None	20% PEG 8000
43	None	None	30% PEG 1500
44	None	None	0.2 *M* Mg formate
45	0.2 *M* Zn acetate	0.1 *M* Na cacodylate pH 6.5	18% PEG 8000
46	0.2 *M* Ca acetate	0.1 *M* Na cacodylate pH 6.5	18% PEG 8000
47	None	0.1 *M* Na acetate pH 4.6	2.0 *M* ammonium sulfate
48	None	0.1 *M* Tris-HCl pH 8.5	2.0 *M* ammonium phosphate
49	1.0 *M* Li sulfate	None	2% PEG 8000
50	0.5 *M* Li sulfate	None	15% PEG 8000

PEG, polyethylene glycol; MPD: 2-methyl-2,4-pentanediol.

Because good-quality crystals are not usually obtained in the first screen, once crystals (most often microcrystals) have been observed in trial experiments, crystallization conditions must be improved for crystal size and quality. At this stage, we usually perform a "grid screen." For each condition, two variables (such as pH and polyethylene glycol [PEG] concentration) are altered in a two-dimensional (x,y) grid. After fine-tuning of all the parameters,

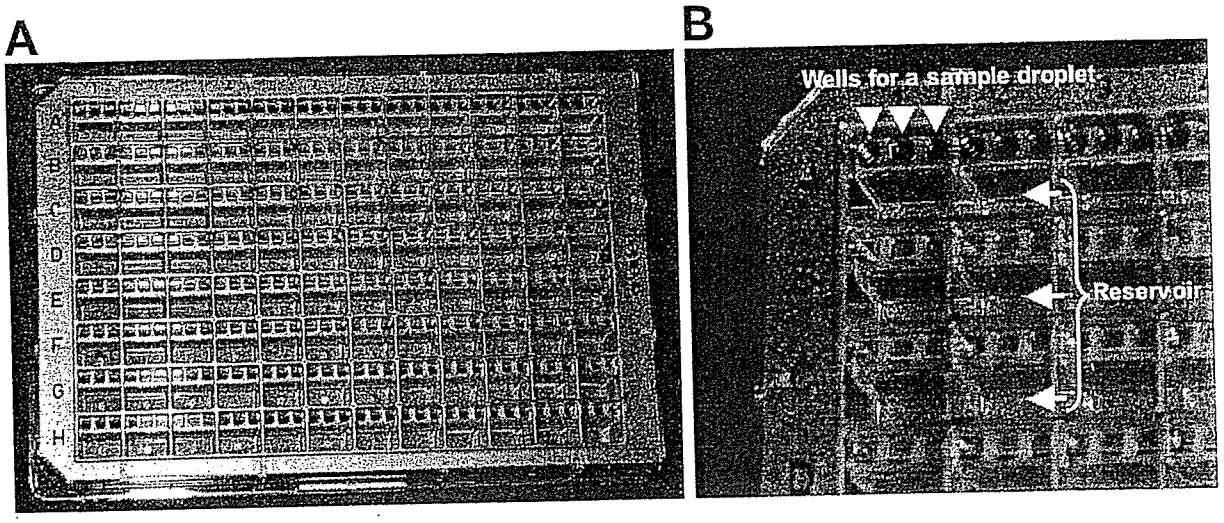

Fig. 2. Greiner CrystalQuick 96-well sitting drop crystallization plate. The plate has 8 vertical wells and 12 horizontal wells. Within each well is a rectangular reservoir with 0.1 mL of fill volume. Adjacent to the reservoir is a ledge containing three drop-support wells for each sample.

crystals suitable for X-ray study are obtained. If the crystals have appropriate size and are really made of protein, not salt, then this is the time to start characterizing them by X-ray diffraction with the help of a protein crystallographer.

2. Materials

2.1. Preparation of Proteins for Crystallization

1. Tris-buffer(TB): 10 m*M* Tris-HCl, pH 7.5 (*see* **Note 2**). Prepared by diluting 100X stock solution (1 *M* Tris-HCl, pH 7.5) with deionized water.
2. Dialysis tubes: Spectra/Por 7 or its equivalent, whose membrane has been treated to minimize the content of heavy metals that can affect crystallization of the protein. Rinse with TB prior to use to remove sodium azide that has been added as a preservative when shipped.
3. Centrifugal filter device: Amicon Ultra-4 (Millipore). There are five devices with different nominal molecular weight limits (NMWLs; 5000, 10,000, 30,000, 50,000, and 100,000). For higher recovery, use a NMWL device with a cutoff range a bit smaller than the molecular weight (MW) of the protein of interest. Prerinse the devices with TB prior to use.

2.2. Initial Screening of Crystallization Conditions

1. Crystal screen: Crystal Screen (Hampton Research) or Crystal Screen Basic (Sigma-Aldrich) containing 50 solutions (*see* **Table 1** and **Note 1**) described in the original sparse matrix by Jancarik and Kim *(8)*.
2. Crystallization plate: Greiner CrystalQuick 96-well sitting drop crystallization plate (Hampton Research; *see* **Fig. 2** and **Note 3**).

3. Sealing tape: a roll of 4-in. wide Crystal Clear Sealing Tape (Hampton Research) or its equivalents. Tapes or films used for sealing crystallization plate should be optically transparent for viewing with a microscope.

3. Methods

Crystallization experiments start with "crystal quality" protein (*see* **Note 4**). Prior to a crystallization experiment, the protein sample should be concentrated in a low-ionic-strength buffer. The crystallization of the protein can be divided into the following two stages: (1) initial screening to obtain any kind of crystals or promising precipitates and (2) optimization to improve the crystals for X-ray diffraction data collections. Ninety-six-well crystallization plates (*see* **Fig. 2** and **Note 2**), which have been developed for sitting drop vapor diffusion to facilitate high-throughput crystallization, are used for both for screens and optimizations. Commercially available "sparse matrix" screens are currently the best choice for initial trials (*see* **Table 1** and **Note 1**). The crystallization experiments are examined daily by observation of the protein droplets using a stereo microscope. The conditions that produce microcrystals should be optimized by "grid screening" to grow high-quality (free of cracks and defects) single crystals of appreciable size (0.05–0.1 mm at least for the dimensions of a face) suitable for X-ray study.

3.1. Preparation of the Proteins for Crystallization

1. Prepare several milligrams of the protein of interest with appropriate purity (*see* **Note 5**).
2. If the protein is lyophilized, dissolve the protein in approx 1 mL of TB (*see* **Note 6**). If the protein is hard to dissolve, then incrementally increase the salt (50, 100, 150, and 200 m*M* NaCl) until it is fully in solution.
3. Dialyze the protein against 1 L of TB (*see* **Note 7**). If the protein is already in solution, start from this step. Change the dialysis solution twice at 6-h intervals. If the sample precipitates, add NaCl in the dialysis solution in order to prevent precipitation, and repeat the step. The salt concentration of the protein sample should be as low as possible. Ideally, it is best to prepare samples in a lower buffer concentration without salt.
4. Remove undisclosed particles by centrifugation (20,000*g* for 10 min).
5. Concentrate the protein solution with a centrifugal filter device Amicon Ultra-4. In general, 10 mg/mL is a good starting protein concentration for initial crystallization trials (*see* **Note 8**). Add the sample to the Amicon Ultra filter unit and spin at a maximum 4000*g* for approx 10–60 min in a swinging-bucket rotor.
6. Recover the concentrated protein by inserting a pipet into the bottom of the filter unit.
7. Store the protein at 4°C until it is used in the crystallization experiment. For longer storage, –70°C is better; however, freezing and rethawing of the sample should be avoided. Therefore, aliquot the protein into several tubes (100–200 µL each) and quick-freeze each one in a liquid nitrogen bath before placing at –70°C.

8. Do not mix different purification batches in crystallization trials. Because it is not uncommon for one batch of protein to crystallize whereas the next will not, it is vital to keep a history of each sample and to track each batch separately.

3.2. Setting Up Protein Drops for Initial Crystallization Screening

1. These instructions assume the use of a Greiner CrystalQuick 96-well sitting drop crystallization plate (**Fig. 2**). Depressions in the plate may be sprayed with pressurized air or some inert gas to blow away dust just before dispensing reservoir solutions. Pipet 0.1 mL of each crystallizing solution of the screen in each of the 96 reservoirs.
2. Pipet 0.5 µL of the protein solution onto the drop-support well of A1 (*see* **Notes 9** and **10**). To carry out crystallization experiments on such a submicroliter scale, it is recommended to use Pipetman P2 (Gilson) or its equivalent.
3. Pipet 0.5 µL of reagent from the reservoir onto the drop-support well of A1 and mix with the protein solution.
4. Repeat **steps 2** and **3** for the remaining reservoirs.
5. Seal the plate with a strip of clear sealing tape.
6. Leave the plate in an incubator, and maintain a fairly constant temperature. Crystallization trials should be performed at a minimum of two temperatures, usually 20 and 4°C, because most protein crystals have been obtained at these temperatures. If possible, try another temperature between 10 and 15°C.
7. The crystallization plates are examined using a stereo microscope (1) immediately after setup, (2) once a day for the first week, and (3) once a week for several weeks (*see* **Note 11**).
8. In wells in which the protein precipitated immediately after making the drop, repeat the setup with modification. Halve the reservoir solution concentration with deionized water and repeat **steps 2–5**. It may slow crystal nucleation.
9. If enough protein sample is left, repeat **steps 1–8** with other screening kits, e.g., Crystal Screen II, PEG/ION Screen, INDEX, SALTRx (Hampton Research), Extension Kit, Low Ionic Kit, PEG Grid Screening Kit (Sigma-Aldrich), Wizard Screens (Emerald BioStructures), and so on. Different screens consist of solutions designed based on different strategies, thus they may compensate for gaps in the original sparse matrix screen *(8)*.

3.3. Observation of the Drops by a Stereo Microscope

1. Scan the drops at about ×20–40 magnification, and when something suspicious appears, increase the magnification to ×80 or ×100 for a better view (*see* **Notes 12** and **13**). Scan the entire depth of the drop, because crystals will form at different levels.
2. Crystals occur in a great variety of shapes such as needles, blades, walnuts, plates, and various geometric shapes and in various sizes (hardly observable 10 µ to 1 mm). An example is shown in **Fig. 3**.
3. Crystals are often distinguished from amorphous substances by their flat faces with sharp edges and by their anisotropy. Anisotropy of the crystals is examined by putting them between a crossed polarizer attached to a stereo microscope. They

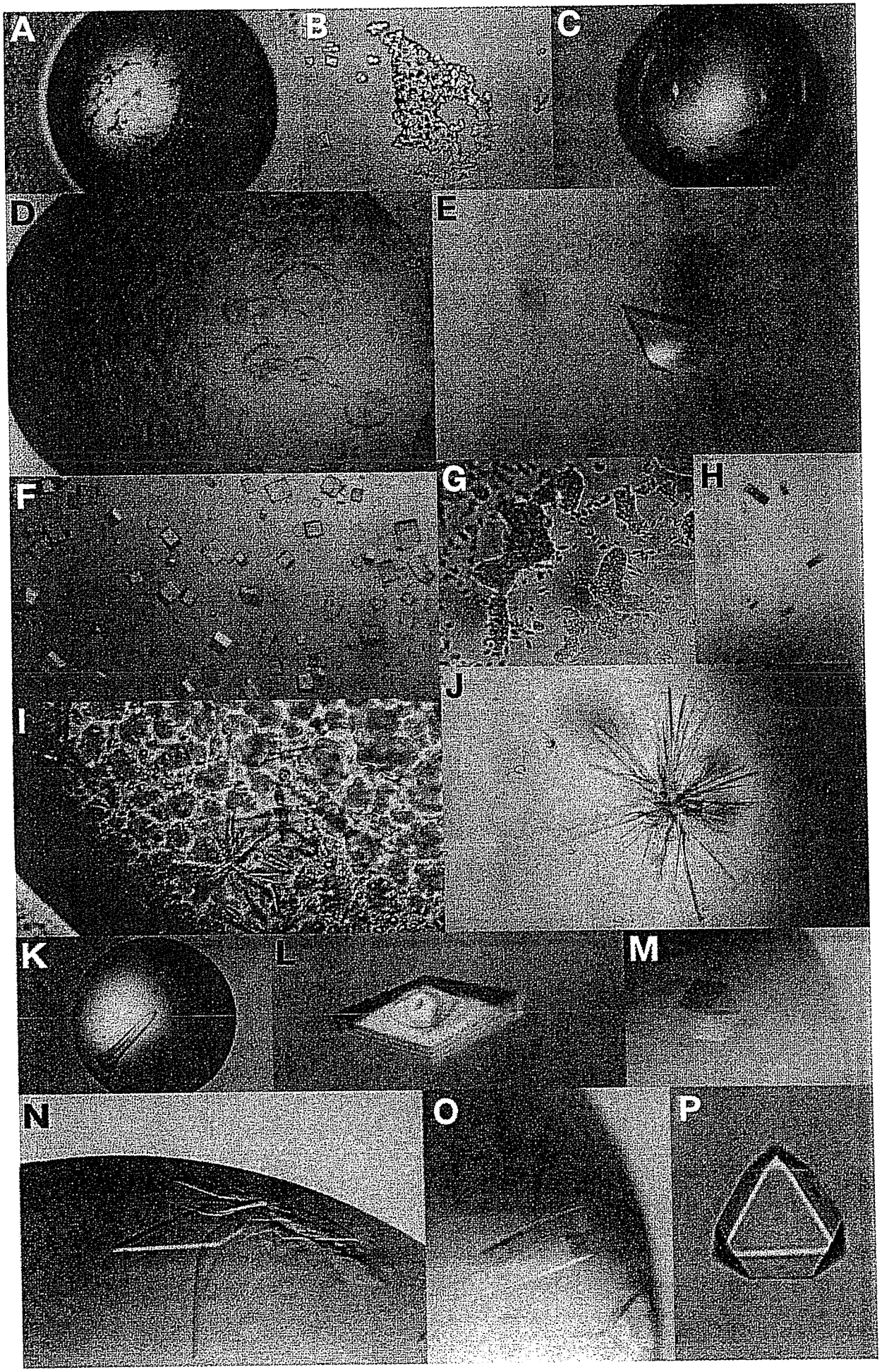

Fig. 3.

sometimes display beautiful colors, because the crystals are birefringent (*see* **Fig. 3C,E,H,L**).

4. Carefully observe everything to be familiar with the differences between microcrystals, amorphous aggregates, and sweater fuzz. If something suspicious is found, make new drops under the same conditions and check its reproducibility. True crystals should be reproduced if the protein is not degraded.
5. When either crystals or micro crystals are found, it is important to verify that the crystals are protein and not salt. IZIT (Hampton Research) is an example of a protein-binding dye. If the crystals obtained are suspected to be salts, a grain of the dye can be added to the drop. Salt crystals will not absorb the dye (*see* **Note 14**).
6. Another method of verifying protein crystals is to take a needle and try to crush the crystals. Salt crystals are so hard to break that one can often hear them snap. Protein crystals are much more fragile and easier to smash.

3.4. Optimization of the Crystallization Conditions

1. Once the crystals (most often microcrystals or suspicious crystals) are obtained in trial experiments, crystallization conditions must be improved for crystal size and quality. pH and precipitant concentration are two of the most important determinants of protein solubility; therefore, they will be the first parameters optimized by a grid screen.
2. Prepare reservoir solutions for the grid screen with variations in pH (in steps of 0.5 pH units initially, then 0.1 pH units finally) vs precipitant concentrations (decreasing in steps of 5%, initially), beginning around the pH value and the precipitant concentration that was found in the initial screen (*see* **Note 15**). Refine those parameters until the optimal crystallization conditions are found.
3. Protein concentration, temperature, and droplet size should also be optimized.
4. Add inhibitors, substrate, or co-factors to the protein drop using the optimized well conditions. Repeat the initial screen with the additive compound if an effect is found (*see* **Note 16**).

Fig. 3. *(Opposite page)* Photo micrographs of the results of crystallization. Crystals or microcrystals of various morphologies obtained from various proteins, including troponin complexes *(9,10)*, in initial crystallization screens are shown in **A**, **B**, **D**, and **F–J**. Transparent spherulite clusters made of tiny crystals were observed (**B**) in a close up view of **A**, suggesting that the well condition was a good starting point for optimization. After optimization of the conditions, single crystals with sharp edges were obtained (**C**) and successfully used for X-ray study. Crystals grown too quickly without edges (**D**) were improved by lowering both the protein and the precipitant concentrations (**E**). Single separated crystals (**K–M**, **O**, and **P**) or single crystals in the cluster of plates (**N**) were obtained after refining the crystallization conditions and were used for diffraction studies. Some crystals, not all, show birefringence (**C**, **E**, **H**, and **L**). Sometimes crystals eventually appear in the oil phase of a drop of salt-polyethylene glycol (PEG)-protein (**I**), because the protein may preferentially partition into the PEG-rich oily phase, thereby becoming locally concentrated enough to nucleate.

5. Repeat **steps 2–4** for other conditions that were not optimized before.
6. Once crystals with the appropriate size are obtained, start to characterize them by X-ray diffraction. For structural studies, it is not morphology but the diffraction quality of the crystals that is important.

4. Notes

1. Although sparse matrix screens are a biased sampling of crystallization parameters, selected from known or published successful crystallization conditions, they are an efficient method to screen a large number of parameters with a limited amount of protein. In our experiences, the first crystals from nearly half of the proteins tested in the initial screens were obtained using such sparse matrix-based ready-made kits. For example, the first crystals of the complexes of troponin, TnC/TnI(1-47) dimer *(9)* and TnT/TnC/TnI trimer *(10)*, were obtained from the solutions no. 38 and no. 17 of Crystal Screen (Hampton Research), respectively.
2. The solution in which the protein is finally dissolved should be as simple as possible (*see* **Note 7**), and 10 m*M* HEPES/NaOH, pH 7.0 is also a common example. It is better not to use phosphate buffers for proteins intended for crystallization even during the preparation procedure, because they often give rise to salt crystals. For proteins susceptible to oxidation, one often needs to add an excess amount of dithiothreitol (~20 m*M*) both in the drop and in the reservoir in order to keep the sample homogeneous (*see* **Note 10**).
3. 96-well plates are much more compact and use less material than 24-well plates, which have been conventionally used. In our experience, there are no obvious differences between the two systems in the results from the initial screens.
4. The protein should be at least 90–95% pure by sodium dodecyl sulfate-polyacrylamide gel electrophoresis (SDS-PAGE) *(11)* and staining with Coomassie Brilliant Blue. Always consider further purification of the protein (1) if the initial screen does not produce any promising results or (2) to improve crystal quality when optimizing. It is our belief that poor purity is the most common cause of unsuccessful crystallization, and the purity requirements of macromolecules must be higher than in other fields of molecular biology. On the other hand, it is not always true that proteins with high purity are easily crystallized. In our case, before truncating the fragile portion of the troponin complex *(10)*, full-length molecules that are extremely pure (more than 99% on SDS-PAGE) would never crystallize. In such cases, try screens with different constructs of varying lengths, different isoforms, or the protein from different sources. Small changes in the physical properties of the proteins can substantially affect its ability to crystallize. Isolated structural domains of proteins are very often easily crystallized with high quality, and limited proteolysis is one of the best methods to figure out which structural domains are suitable for crystallization experiments *(12)*.
5. The initial gels prior to the crystallization experiments are important for documentation of the homogeneity of the protein, possible batch variations, and for verification of protein stability. As proteins degrade with time, comparison of the gels from failed crystallization drops with the original ones will establish if the protein

has deteriorated. Aging results from the action of contaminants either already present or introduced into the samples or from modifications generated by oxidants. In some cases, changes in crystal formation are owing to the presence of fungi or mold that multiply in the stored protein solutions. Store solutions in airtight bottles to prevent contamination by airborne micro-organisms and wear gloves during manipulations; fingers are always contaminated by proteases and bacteria that may degrade the proteins.

6. Handle the protein solution gently. When mixing a lyophilized sample into solution or thawing a sample, one should take care not to make foam, because foam can be a sign of denaturation.
7. Dialysis will remove nonvolatile buffers and other chemicals that may have been present either before lyophilization or in the solution of the final purification step. Sometimes trace amounts of impurities can affect the ability of proteins to crystallize. The buffer concentration of the sample solution (10 m*M*) is 10 times lower than the buffer concentration in the reservoir solutions of the screens, which usually contain 100 m*M* of buffer. Hence, the pH of the crystallization drops becomes closer to that of the reservoirs, which allows the screens to be more effective.
8. For obtaining the protein concentration, spectrophotometry is an accurate and easy method. Theoretical molar absorption coefficients ε of polypeptides can be calculated from the content of tryptophan and tryrosine using:

$$\varepsilon_{280\text{nm}} = 5500n_x + 1490n_y,$$

where 5500 and 1490 are the good estimates of the molecular absorption coefficients for tryptophan and tyrosine residues in proteins at 280 nm *(13)*, and n_x and n_y are the numbers of those residues, respectively. Thus, protein concentration is obtained from:

$$c\ (\text{mg/mL}) = A_{280\text{nm}} \times \varepsilon_{280\text{nm}}/M_r\ (M_r\text{; molecular weight of the protein})$$

9. Before a crystallization experiment, solid particles such as dust, denatured proteins, and solid contaminants from purification columns should be removed. This can be achieved simply by centrifugation (20,000*g* for 5 min) immediately prior to setting up the crystallization trials.
10. It is better to make drops as small as possible. Saving the sample allows screening of more conditions. In addition, there is a great advantage in that a smaller drop reaches equilibrium faster, resulting in faster crystallization. One of our proteins crystallizes within a day from a drop consisting of 0.3 µL of protein and 0.3 µL of reservoir solution, however is never crystallizes from the larger drops. After solving structure, it turned out that the protein was oxidized to form a disulfide bond between two of three neighboring cysteine residues within a few days, resulting in sample heterogeneity that prevented crystallization (*see* **Note 2**).
11. When the storage space is large enough for the plates, the experiment may be continued for as long as 1 yr. Because the crystallization plates are made of polystyrene that allows for some evaporation overtime, this long-term storage can eventually result in crystallization.

12. The stereomicroscope should have an observation platform large enough to support the crystallization plate when looking at all the drops. It is better to have transmitted light with a separate light source connected with an optical fiber in order to prevent heating the base, because crystals can be dissolved easily by temperature variation.
13. It is highly recommended to use a microscope with a higher magnification lens (~×100) because it is sometimes very difficult to distinguish microcrystals and amorphous precipitates using microscopes with lower magnification (~×50). We use the Leica MZ-16 stereo microscope for viewing drops. If a stereo microscope with a high magnification lens is not available, a standard microscope with a ×10 objective lens and ×10 eyepieces for a better view may be used.
14. In protein crystals, the molecules are loosely packed with large solvent-filled channels that normally occupy 40–60% of the crystal volume. This is an advantage when reacting the protein with small reagent molecules such as dyes or heavy metal compounds to be used for phasing, because they can diffuse through these channels and reach reactive sites in the all the protein molecules in the crystal.
15. It is important to find the threshold at which the protein starts to precipitate, because nucleation of crystals usually occurs close to this point, and crystals grow under the supersaturated condition.
16. Inhibitors, substrates, or co-factors (coenzymes) induce some conformational changes in proteins upon binding, and this might result in a more compact and stable state. The apoprotein and protein–ligand complex may be sufficiently different in solubility and physical behavior in many cases. Thus, this may provide a second or third chance at growing crystals unless one does not have any crystals from the apoprotein. In addition, such a complex is inherently more interesting than the apoprotein alone when the structure is eventually determined.

References

1. Drenth, J. (1994) *Principles of Protein X-Ray Crystallography.* (Cantor, C.R., ed.), Springer-Verlag, New York.
2. Blundell, T. L. and Johnson, L. N. (eds.) (1976) *Protein Crystallography.* Academic, Inc., San Diego.
3. Blow, D. (ed.) (2002) *Outline of Crystallography for Biologists.* Oxford University Press, New York.
4. Ducruix, A. and Giege, R. (eds.) (1999) *Crystallization of Nucleic Acids and Proteins: A Practical Approach.* Oxford University Press, New York.
5. McPherson, A. (ed.) (1999) *Crystallization of Biological Macromolecules.* Cold Spring Harbor Laboratory, New York.
6. Terese, M. B. (ed.) (1999) *Protein Crystallization: Techniques, Strategies, and Tips.* International University Line, La Jolla.
7. McRee, D. E. (ed.) (1999) *Practical Protein Crystallography.* Academic, San Diego.
8. Jancarik, J. and Kim, S. H. (1991) Sparse matrix sampling: a screening method for crystallization of protein. *J. Appl. Cryst.* **24,** 409–411.

9. Vassylyev, D. G., Takeda, S., Wakatsuki, S., Maeda, K., and Maeda, Y. (1998) Crystal structure of troponin C in complex with troponin I fragment at 2.3-A resolution. *Proc. Natl. Acad. Sci. USA* **95,** 4847–4852.
10. Takeda, S., Yamashita, A., Maeda, K., and Maeda, Y. (2003) Structure of the core domain of human cardiac troponin in the Ca(2+)-saturated form. *Nature* **424,** 35–41.
11. Laemmli, U. K. (1970) Cleavage of structural proteins during the assembly of the head of bacteriophage T4. *Nature* **227,** 680–685.
12. Takeda, S., Kobayashi, T., Taniguchi, H., Hayashi, H., and Maeda, Y. (1997) Structural and functional domains of the troponin complex revealed by limited digestion. *Eur. J. Biochem.* **246,** 611–617.
13. Pace, C. N., Vajdos, F., Fee, L., Grimsley, G., and Gray, T. (1995) How to measure and predict the molar absorption coefficient of a protein. *Protein Sci.* **4,** 2411–2423.

tapraid4/zh8-bloo/zh8-bloo/zh800407/zh80803d07g | sangreyj | S=4 | 12/9/06 | 19:57 | Art: 2006/029298 | Input-DCT-???
Collection Codes: 11
DOI: 10.1182/blood-2006-06-029298
HEMOSTASIS, THROMBOSIS, AND VASCULAR BIOLOGY

Receptor activator of nuclear factor (NF)–κB ligand (RANKL) increases vascular permeability: impaired permeability and angiogenesis in eNOS-deficient mice

Jeong-Ki Min, Young-Lai Cho, Jae-Hoon Choi, Yonghak Kim, Jeong Hun Kim, Young Suk Yu, Jaerang Rho, Naoki Mochizuki, Young-Myeong Kim, Goo Taeg Oh, and Young-Guen Kwon

[1]Department of Biochemistry, College of Sciences, Yonsei University, Seoul, Republic of Korea; [2]Department of Molecular and Cellular Biochemistry, School of Medicine, Kangwon National University, Chunchon, Kangwon-Do, Republic of Korea; [3]Department of Ophthalmology, Seoul National University College of Medicine, Seoul National University Hospital, Seoul, Republic of Korea; [4]Seoul Artificial Eye Center, Clinical Research Institute, Seoul National University Hospital, Republic of Korea; [5]Department of Structural Analysis, National Cardiovascular Center Research Institute, Osaka, Japan; [6]Department of Microbiology College of Natural Sciences, Chungnam National University, Daejeon, Republic of Korea; [7]Division of Molecular Life Science, Ewha Womans University Seoul, Republic of Korea

Receptor activator of nuclear factor (NF)–κB ligand (RANKL) is emerging as an important regulator of vascular pathophysiology. Here, we demonstrate a novel role of RANKL as a vascular permeability factor and a critical role of endothelial nitric oxide synthase (eNOS) in RANKL-induced endothelial function. RANKL increased the vascular permeability and leukocyte infiltration in vivo and caused the breakdown of the blood-retinal barrier in wild-type mice but not in eNOS-deficient mice. In vitro, it increased endothelial permeability and reduced VE-cadherin–facilitated endothelial cell-cell junctions in a NO-dependent manner. RANKL also led to the activation of Akt and eNOS and to NO production in endothelial cells (ECs). These effects were suppressed by the inhibition of TRAF6, phosphoinositide 3′-kinase (PI3K), Akt, or NOS by genetic or pharmacologic means. Inhibition of the TRAF6-mediated NO pathway reduced EC migration and capillary-like tube formation in response to RANKL. Moreover, the effects of RANKL on ECs sprouting from the aorta, and neovessel formation in both the mouse Matrigel plug assay and corneal micropocket assay, were impaired in eNOS-deficient mice. These results demonstrate that RANKL promotes vascular permeability and angiogenesis by stimulating eNOS by a TRAF6-PI3K-Akt–dependent mechanism. These properties may be relevant to the pathogenesis of angiogenesis-dependent and inflammatory vascular diseases. (Blood. 2007;109:000-000)

Introduction

Angiogenesis, the formation of new blood vessels from a preexisting vascular bed, is a pivotal process not only in embryonic development but also in the progression of a variety of pathologic conditions.[1] A large number of molecules, which are composed of growth factors, cytokines, and lipid metabolites, are shown to be involved in pathophysiologic neovascularization by stimulating endothelial cells (ECs) directly or indirectly.[2] Some of these factors, including VEGF, often possess their abilities to increase vascular permeability and thus contribute to deteriorating tissue damage.

Receptor activator of nuclear factor (NF)–κB ligand (RANKL), also known as ODF, TRANCE, and OPGL, has well-understood roles in the skeletal and immune systems in which it induces osteoclast differentiation from hematopoietic precursors and regulates the function and survival of dendritic cells.[3] Recently, interest has grown in its physiologic and pathologic relevance to vascular biology.[4] Mounting evidence suggests that RANKL and its decoy receptor, osteoprotegrin (OPG), participate in multiple aspects of vascular calcification; for example, mice lacking OPG suffer late medial calcification of the renal and aortic arteries in addition to early onset osteoporosis.[5-7] Moreover, a role for the OPG/RANKL/RANK axis in atherogenesis and plaque destabilization has been recently reported.[8] OPG inactivation accelerates advanced atherosclerotic lesion progression and calcification in older ApoE mice.[9] TRANCE is strongly expressed in vascular cells in vitro, as well as in vivo. OPG and it are induced by inflammatory cytokines in human endothelial cells (ECs), although with different temporal profiles.[10] In vivo, RANKL is present in the small blood vessels of the skin and in arterial smooth muscle cells,[11] and it appears to be up-regulated in atherosclerotic lesions, calcified vessels, and valves.[4,6,9] Moreover, the RANKL receptor, RANK, is also expressed in ECs of the rat coronary artery and developing blood vessels of the rat embryo in vivo, as well as in freshly isolated human umbilical vein ECs (HUVECs).[12] In agreement with these patterns of expression, RANKL stimulates the survival of cultured ECs and their production of inflammatory cell adhesion molecules; it also promotes in vitro angiogenesis by the ECs and elicits neoangiogenesis in animal models.[13] Moreover, VEGF increases RANK mRNA and protein in ECs, augmenting their angiogenic response to RANKL.[12] Therefore, the RANKL/RANK/OPG system is believed to be an important link between the vascular, skeletal, and immune systems.

Endothelium-derived nitric oxide (NO), originally identified as endothelium-derived relaxing factor, promotes angiogenesis and

Submitted June 14, 2006; accepted September 29, 2006. Prepublished online as *Blood* First Edition Paper, October 12, 2006; DOI 10.1182/blood-2006-06-029298.

The online version of this article contains a data supplement.

The publication costs of this article were defrayed in part by page charge payment. Therefore, and solely to indicate this fact, this article is hereby marked "advertisement" in accordance with 18 USC section 1734.

plays an important role in vascular remodeling and the maintenance of vascular integrity.[14,15] In ECs, NO is a product of the conversion of L-arginine to citrulline by endothelial NO synthase (eNOS). eNOS produces low levels of NO constitutively but can be transiently stimulated to produce high levels by various hormones and environmental stimuli such as vascular endothelial growth factor (VEGF), angiopoietin-1 (Ang-1), shear stress, and hypoxia.[16,17] Moreover, eNOS knockout (KO) mice exhibit impaired postnatal angiogenesis in response to tissue ischemia.[15,16] Although the mechanisms by which it promotes angiogenesis is not fully elucidated, NO has emerged as an important modulator of endothelial activation underlying physiologic and pathologic angiogenesis and inflammation.

The increased expression of RANKL in the injured blood vessels suggests the involvement of RANKL in vascular pathophysiology. However, little information is available for its vascular function and underlying signaling mechanisms in ECs. In the present study, our data demonstrate that RANKL has a significant effect on vascular permeability, which is governed by interendothelial junctions between adjacent cells. We further present genetic and pharmacologic evidence that endothelium-derived NO plays a critical role in promoting the vascular permeability and angiogenesis induced by RANKL.

Materials and methods

Cell culture and reagents

HUVECs were isolated from human umbilical cord veins by collagenase treatment, as described previously,[18] and were used in passages 2 to 7. They were grown in M199 medium (Invitrogen, Carlsbad, CA) supplemented with 20% fetal bovine serum (FBS). Soluble RANKL (hCD8-conjugated form) was purified from insect cells as described previously.[15]

Endothelial-cell migration assay

Chemotactic motility of HUVECs was assayed as described previously.[19] Briefly, the lower surface of the filter was coated with 10 μg gelatin. Fresh M199 medium (1% FBS) containing RANKL was placed in the lower wells. The cells were trypsinized and suspended at a final concentration of 1×10^6 cells/mL in M199 containing 1% FBS. One hundred microliters of the cell suspension was loaded into each of the upper wells, and the chamber was incubated at 37°C for 4 hours. The cells were fixed and stained with hematoxylin and eosin. Nonmigrating cells on the upper surface of the filter were removed by wiping with a cotton swab, and chemotaxis was quantified with an optical microscope (× 200) by counting cells that had migrated to the lower side of the filter. Ten fields were counted for each assay.

Tube formation assay

Tube formation was assayed as previously described.[19] Briefly, 250 μL growth factor-reduced Matrigel (10 mg protein/mL) was pipetted into a 16-mm diameter tissue culture well and polymerized for 30 minutes at 37°C. HUVECs incubated in M199 containing 1% FBS for 6 hours were harvested after trypsin treatment, resuspended in M199, plated onto the layer of Matrigel at a density of 1.8×10^5 cells/well, and RANKL was added. After 20 hours, the cultures were photographed (× 200). The area covered by the tube network was measured using an optical imaging technique in which pictures of the tubes were scanned in Adobe Photoshop (San Diego, CA) and quantified with Image-Pro Plus (Media Cybernetics, Silver Spring, MD).

Retroviral vectors and generation of stable transfectants

cDNA sequences encoding hemagglutinin (HA)–tagged dominant-negative TRAF2 (DN-T2) and Flag-tagged dominant-negative TRAF6 (DN-T6) were subcloned into pMSCVpuro vector (Clontech, Palo Alto, CA) and introduced into HEK293T cells (packaging cell line) with 1 μg pVSV-G vector (Clontech) using LipofectAMINE Plus reagent according to the manufacturer's instructions. The next day, the virus in the supernatants of these cells was added to HUVECs along with 5 μg/mL polybrene. After 24 hours of incubation, the medium was removed and replaced with fresh medium containing 3 μg/mL puromycin. Puromycin-resistant clones were selected by incubating for 1 week in the presence of 3 μg/mL puromycin. Protein expression was confirmed by Western blotting.

[^{3}H] Sucrose permeability assay

HUVECs were plated onto a Transwell filter (Corning Costar, Acton, MA). After reaching confluence, HUVECs were incubated with M199 containing 1% FBS for 3 hours and treated with various concentrations of RANKL (0.5, 1, and 5 μg/mL) or 20 ng/mL VEGF for 1 hour. Fifty microliters (0.8 μCi [0.0296 MBq]/mL) of [^{3}H]sucrose (1 μCi [0.037 MBq]/μL; Amersham Pharmacia, Piscataway, NJ) was added to the upper compartment. The amount of radioactivity that diffused into the lower compartment was determined after 30 minutes by liquid scintillation counter (Wallac, Gaithersburg, MD; PerkinElmer, Wellesley, MA).

Miles vascular permeability assay

Miles assay was performed as described previously.[20] Evans blue dye (100 μL of a 1% solution in 0.9% NaCl) was injected into the tail vein of C57BL/6 wild-type (WT) and eNOS knockout (KO) mice (n = 7 per group). After 10 minutes, RANKL (10 μg in 10 μL PBS) was injected intradermally into the shaved back skin of mice. After 20 minutes, the animals were killed, and an area of skin that included the blue spot resulting from leakage of the dye was removed. Evans blue dye was extracted from the skin by incubation with formamide for 4 days at room temperature, and the absorbance of the extracted dye was measured at 620 nm with a spectrophotometer.

Perfusion of FITC-dextran

C57BL/6 WT and eNOS KO mice (8-10 weeks old, n = 7 per group) were examined for vascular leakage after injection of RANKL. RANKL (10 μg) or PBS was injected slowly into the vitreous cavity. After 24 hours, the mice were deeply anaesthetized using ketamine/xylazine and received an intravenous injection of 10 mg FITC-dextran (MW = 20 000 D; Sigma, St Louis, MO). After 30 minutes, the eyes were enucleated and immediately fixed in 4% paraformaldehyde. The retinas were dissected out, cut in a Maltese cross configuration, flat-mounted on glass slides, and viewed with a fluorescence microscope (Zeiss, Jena, Germany). The vascular permeability was quantified by counting sites with extravasation of fluorescence at postcapillary vessel.

VE-cadherin translocation assay

HUVECs plated in 6-well plates were serum starved in medium 199 containing 1% FBS for 6 hours. They were then stimulated with 5 μg/mL RANKL for 1 hour and fractionated in cytoskeleton-stabilizing buffer (10 mM HEPES [pH 7.4], 250 mM sucrose, 150 mM KCl, 1 mM EGTA, 3 mM $MgCl_2$, 1 × protease inhibitor cocktail [Roche Diagnostics, Indianapolis, IN], 1 mM Na_3VO_4, 0.5% Triton X-100) by centrifugation at 15 000*g* for 15 minutes. The proteins in the Triton X-100–insoluble and insoluble fractions were analyzed by Western blotting.

Measurement of nitrite plus nitrate

Production of nitrite plus nitrate (NOx) was measured by the ozone-chemiluminescence method. Culture media from HUVECs were collected and assayed for NOx using a chemiluminescent NO analyzer

tapraid4/zh8-bloo/zh8-bloo/zh800407/zh80803d07g | sangreyj | S=4 | 12/9/06 | 19:57 | Art: 2006/029298 | Input-DCT-???

(Antek Instruments, Houston, TX),[21] and quantified with sodium nitrate as standard.

eNOS activity assay

HUVECs were detached with PBS/EDTA (1 mM) and homogenized in 10 mM Tris-HCl pH 7.4. [^{3}H]-L-arginine to [^{3}H]-L-citrulline conversion was measured with 1 mM $CaCl_2$ with or without L-NAME (1 mM) using a NOS assay kit (Calbiochem, La Jolla, CA).

In vivo Matrigel plug assay

Matrigel plug assays were performed as previously described.[22] Briefly, WT and eNOS KO mice (n = 7 per group) were injected subcutaneously with 0.6 mL Matrigel containing RANKL and 15 U heparin. The injected Matrigel rapidly formed a single, solid gel plug. After 7 days, the skin of the mouse could be easily pulled back to expose the Matrigel plug, which remained intact. Hemoglobin was measured by the Drabkin method with Drabkin reagent kit 525 (Sigma) to quantify blood vessel formation. The concentration of hemoglobin was calculated from a known amount of hemoglobin assayed in parallel. To identify infiltrating endothelial cells, immunohistochemistry was performed with anti-CD31 antibody.

Aortic ring assay

Aortas were harvested from 6-week-old male Sprague Dawley rats, 6- to 8-week-old C57BL/6 wild-type (WT), and eNOS knockout (KO) mice. Plates (48-well) were coated with 100 μL Matrigel, and, after it had gelled, the rings were placed in the wells and sealed in place with an overlay of 40 μL Matrigel. RANKL and inhibitors were added to the wells in a final volume of 200 μL human endothelial serum-free medium (Invitrogen). On day 6, cells were fixed and stained with Diff-Quick. The assays were scored, double blind, from 0 (least positive) to 5 (most positive). Each data point was assayed in sextuplet.

Mouse corneal angiogenesis assay

Eight-week-old male C57BL/6 WT and eNOS KO mice (n = 7 per group) were used. After systemic and local eye anesthesia, a central, intrastromal linear keratotomy approximately 0.6 mm in length was performed with a surgical blade, and a micropocket was dissected toward the temporal limbus with a modified von Graefe knife. A sucrose aluminum sulfate pellet coated with Hydron polymer containing control buffer or RANKL (10 μg/pellet) was positioned 0.6 to 0.8 mm from the corneal limbus. On postoperative day 6, we measured the arc of the corneal circumference occupied by angiogenesis (circumferential angiogenesis, in degrees) and vessel lengths and numbers.

Leukocyte infiltration

Eight-week-old male C57BL/6 WT and eNOS KO mice were anesthetized and received a topical application of RANKL (3 μg/mL) or PBS. Twenty-four hours after RANKL application, the retroorbital venous sinus of each animal was injected intravenously with 200 μL biotinylated *Lycopersicon esculentum* lectin (1 mg/mL; Vector Laboratories, Burlingame, CA), which binds to *N*-acetyl-D-glucosamine residues on the luminal surface of vascular endothelial cells.[23] To perfuse the mice, the chest cavity was opened, and the atria were cut to allow outflow of blood and perfusate. Mice were perfused with a fixative (1% paraformaldehyde, 0.5% glutaraldehyde in PBS) via the left ventricle. The ears were removed, and the vascular architecture was analyzed in whole mounts of mouse ears, using a ZEISS AxioSkop2 microscope. Images of blood vessels and infiltrated leukocytes were captured, using a ZEISS AxioCam.

Statistical analysis

Data are presented as mean ± SD or ± SE. Statistical comparisons between groups were performed using one-way ANOVA followed by Student *t* test.

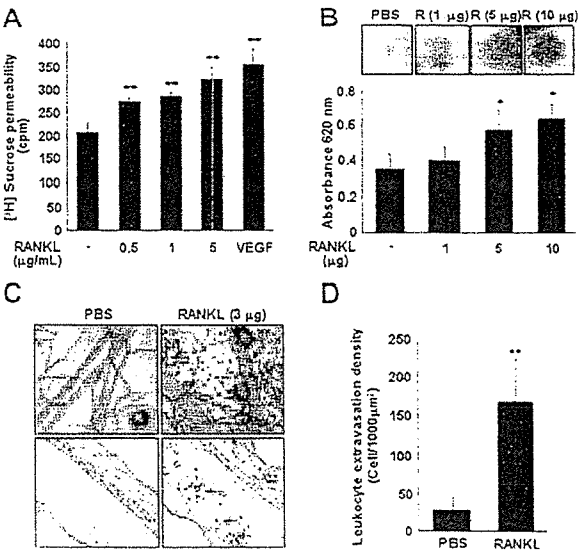

Figure 1. RANKL induces vascular hyperpermeability and leukocyte extravasation. (A) An in vitro [^{3}H]sucrose permeability assay was performed as described in "Materials and methods." Three independent experiments were performed in duplicate. Data are means ± SEs; $^{**}P < .01$ versus untreated control. (B) In vivo Miles vascular permeability assay. Various concentrations of RANKL (R) or PBS were injected intradermally into the skin of C57BL/6 mice (n = 7 per group) after intravenous injection of Evans blue. Representative picture (top) and quantity (bottom) of extravasated Evans blue in the mouse skin. Data are means ± SDs; $^{*}P < .05$ versus PBS. (C) Leukocyte extravasation. Twenty-four hours after RANKL (3 μg) application as described in "Materials and methods," mice (n = 5 per group) were perfused with the lectin *L esculentum* to visualize extravasated leukocytes (top). This experiment was performed twice. Leukocytes in the ear sections were immunostained with anti-CD11a antibody (bottom). Arrows indicate extravasated CD11a$^+$ leukocytes. (D) Quantitative analysis of extravasated leukocytes. Data are means ± SDs; $^{**}P < .01$ versus PBS.

Results

RANKL induces vascular hyperpermeability and leukocyte extravasation

Human CD8-conjugated soluble RANKL increased [^{3}H] sucrose diffusion through the pores of Transwell membranes in HUVEC monolayer culture in a dose-dependent manner (Figure 1A). The near maximal activity at 5 μg/mL was comparable to that achieved with 20 ng/mL VEGF. To test whether RANKL induces vascular hyperpermeability in vivo, a modified Miles vascular permeability assay was performed using intravenous injection of Evans blue followed by intradermal injection of RANKL. RANKL strongly induced vascular hyperpermeability in the mouse skin, as shown by the increased leakage of Evans blue (Figure 1B). Spectrophotometric measurements of the extravasated Evans blue revealed that the increase was dose dependent (Figure 1B). We further investigated the effect of RANKL on leukocyte extravasation in vivo. The mice received an ear inoculation of vehicle or RANKL for 24 hours, and then leukocyte infiltration was monitored by in vivo perfusions with the lectin *L esculentum*. RANKL-treated mice showed a dramatic increase in leukocyte extravasation, as compared with vehicle-treated mice (Figure 1C). The identity of extravasated leukocytes was confirmed by CD11a staining in the ear section (Figure 1D).

Impairment of RANKL-induced vascular hyperpermeability in eNOS-deficient mice

The role of endothelial NO in RANKL-induced vascular permeability was evaluated. The NO synthase inhibitor NMA

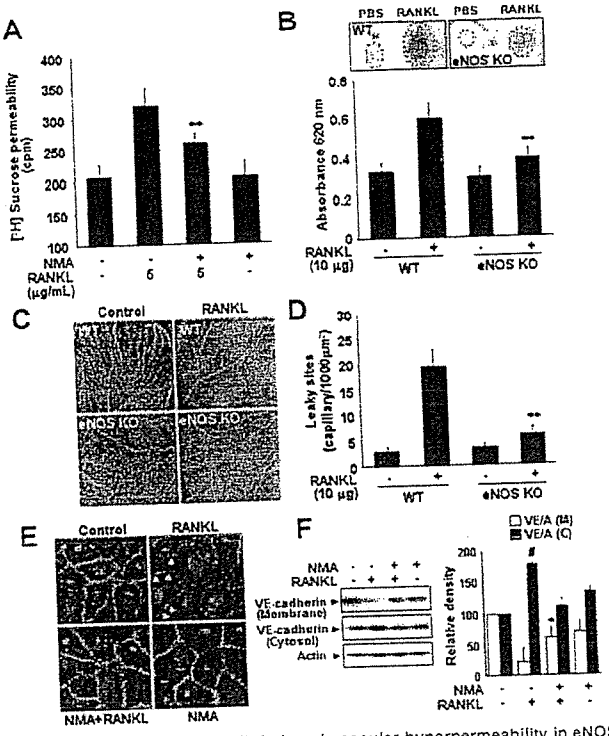

Figure 2. Impairment of RANKL-induced vascular hyperpermeability in eNOS-deficient mice. (A) HUVECs were preincubated for 30 minutes with or without NMA (1 mM) and stimulated with 5 μg/mL RANKL for 1 hour. A [³H]sucrose permeability assay was then performed. Three independent experiments were performed in duplicate. Data are means ± SEs; $^{**}P < .01$ versus RANKL alone. (B) An in vivo Miles vascular permeability assay was performed in WT and eNOS KO mice (n = 7 per group) as described in Figure 1. Data are means ± SDs; $^{**}P < .01$ versus RANKL in eNOS KO. (C) Representative fluorescence images of retinal vessels. RANKL (10 μg) or PBS was injected into the vitreous cavity of WT and eNOS KO mice (n = 7 per group). After 24 hours, the mice received an intravenous injection of 10 mg FITC-dextran (MW = 20 000 D), and their retinas were flat-mounted. (D) The vascular permeability was quantified by counting sites with extravasation of fluorescence at postcapillary vessel. Data are means ± SDs; $^{**}P < .01$ versus RANKL in eNOS KO. (E-F) HUVECs were preincubated for 30 minutes with or without NMA (1 mM) and stimulated with 5 μg/mL RANKL for 1 hour. (E) An immunofluorescence analysis of VE-cadherin. (F) Translocation of VE-cadherin was assessed as described in "Materials and methods." The Triton X-100–insoluble and soluble fractions were subjected to SDS–polyacrylamide gel electrophoresis (PAGE) followed by Western blot analysis with anti–VE-cadherin. Blots are representative of 3 independent experiments. Densitometric analyses are presented as the relative ratio of VE-cadherin to actin. VE indicates VE-cadherin; A, actin; M, membrane; C, cytosol. Data are means ± SDs; $^{*}P < .05$ versus RANKL alone; $^{\#}P < .05$ versus untreated control.

significantly abrogated RANKL-induced endothelial permeability in vitro (Figure 2A). Consistently, vascular hyperpermeability of the mouse skin by RANKL was substantially impaired in the eNOS KO mice compared with WT mice (Figure 2B). We further investigated the role of eNOS in retinal vascular permeability that is caused by breakdown of tight junctions between the retinal vascular endothelial cells. As shown in Figure 2C-D, injection of RANKL into the vitreous cavity of WT mice induced marked retinal vascular leakage as evidenced by the widespread, diffuse fluorescence. By contrast, the retinal vessels of the eNOS KO mice remained clearly delineated, with little or no leakage. Furthermore, the effect of RANKL on leukocyte extravasation in vivo was significantly abrogated in eNOS KO mice compared with WT mice (Figure S1A-B, available on the *Blood* website; see the Supplemental Figures link at the top of the online article).

Vascular endothelial permeability is maintained by the endothelial junction proteins, VE-cadherin, and occludin.[24] The effect of RANKL on adherens junction (AJ) formation was examined by immunostaining with anti–VE-cadherin. In confluent ECs, VE-cadherin is located at cell-cell contacts. When HUVECs were treated with RANKL, the level of VE-cadherin at cell-cell junctions markedly decreased, and pretreatment with NMA blocked this effect (Figure 2E). Normally, VE-cadherin that is anchored to the actin cytoskeleton is detected in the detergent-insoluble fractions of cell lysates.[25] There was a decrease in VE-cadherin in the Triton X-100–insoluble fraction and a concomitant increase in the Triton X-100–soluble fraction after stimulation with RANKL. This effect was reversed by NMA (Figure 2F). Taken together, these results demonstrate that RANKL induces vascular hyperpermeability in an NO-dependent manner by promoting the breakdown of endothelial AJs.

RANKL induces eNOS activation and NO production via a TRAF6/PI3K/Akt signaling pathway

To confirm whether RANKL stimulates NO production in endothelial cells, quiescent HUVECs were stimulated with RANKL and assayed for NO production and eNOS activity. RANKL increased NO production and eNOS activity (Figure 3A-B), without affecting the expression of eNOS protein (Figure 3C). The eNOS activity was evidently increased at 0.5 hours after RANKL treatment and sustained up to 24 hours (Figure 3B). eNOS is an isoform of NO

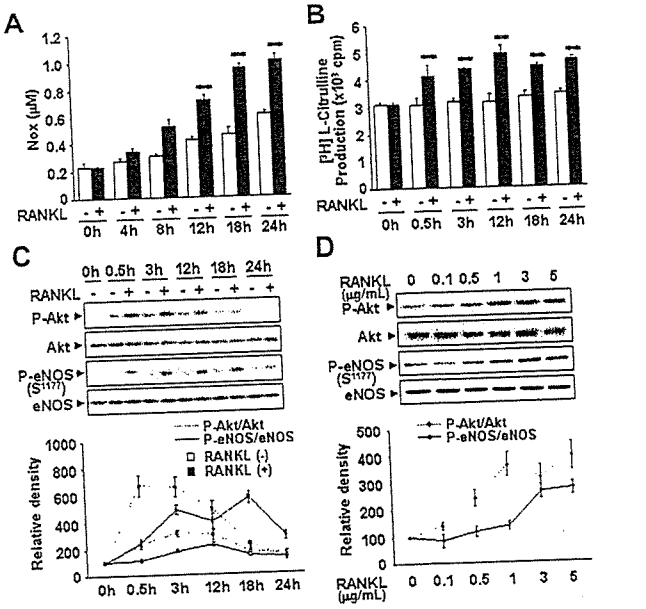

Figure 3. RANKL induces eNOS activation and NO production in endothelial cells. (A-D) HUVECs were stimulated with 5 μg/mL RANKL for the indicated times (A-C) and with various concentrations of RANKL for 30 minutes (D). (A) Levels of NOx was determined in the culture medium by using a chemiluminescent NO analyzer. (B) The eNOS enzymatic activity was measured by the production of [³H]-L-citrulline from [³H]-L-arginine. Three independent experiments were performed in duplicate. Data are means ± SEs. Statistical analysis of the results was carried out using ANOVA. $^{**}P < .01$ versus untreated control in 0 hour and each time point. (C-D) The levels of eNOS protein and phosphorylation of Akt and eNOS by RANKL were determined by Western blotting (top). Blots are representative of 3 independent experiments. Densitometric analyses are presented as the relative ratio of P-Akt to Akt and P-eNOS to eNOS. The relative ratio in untreated control is arbitrarily presented as 100 (bottom).

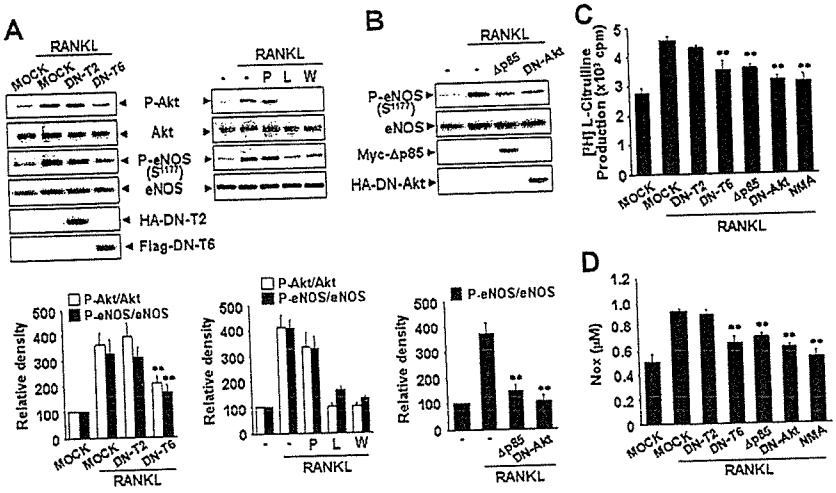

Figure 4. RANKL induces eNOS activation and NO production via a TRAF6/PI3K/Akt signaling pathway. (A) HUVECs were stably transfected with a HA-tagged DN-T2 and a Flag-tagged DN-T6 using retroviral system (left). HUVECs were preincubated for 30 minutes with or without 5 μM PP1, 100 nM Wortmannin, or 1 mM NMA prior to stimulation with RANKL (5 μg/mL) for 20 minutes (right). (B) HUVECs were transiently transfected with a HA-tagged DN-Akt or a Myc-tagged Δp85. (A-B) The levels of eNOS protein and the phosphorylation of Akt and eNOS by RANKL were determined by Western blotting (top). Blots are representative of 3 independent experiments. Densitometric analyses are presented as the relative ratio of P-Akt to Akt and P-eNOS to eNOS (bottom). (C-D) eNOS activity and NO production were measured as described in Figure 3A-B. Three independent experiments were performed in duplicate. Data are means ± SDs: $^{**}P < .01$ versus RANKL alone.

synthase that is constitutively expressed in HUVECs and activated by Akt-mediated phosphorylation at Ser1177.[26,27] When HUVECs were exposed to RANKL, there was a dose-dependent increase in phosphorylation of eNOS at Ser1177 (Figure 3D). The increase was detected within 10 minutes, reached a maximum at 20 to 30 minutes, and was sustained for nearly 24 hours (Figure 3C). Consistent with this, we detected an increase in Akt phosphorylation (Figure 3C-D). However, other phosphorylation sites of eNOS were not changed by RANKL treatment (Figure S2).

We further analyzed the signaling mechanism involved in RANKL-induced eNOS phosphorylation and NO production. RANK, like other TNFR family members, lacks catalytic activity and interacts with TRAFs that act as adaptors activating downstream signaling pathways. Of the TRAFs, TRAF2 and TRAF6 appear to be important components of the RANKL signaling pathway.[28] Overexpression of DN-T6 resulted in substantial inhibition of eNOS phosphorylation, eNOS activity, and NO production, whereas DN-T2 had no effect (Figure 4A,C-D). Recruitment of TRAF6 to the cytoplasmic domains of RANK can lead to the activation of PI3K that subsequently links to Akt pathway. Indeed, the PI3K inhibitors, LY294002 and Wortmannin, markedly inhibited RANKL-induced eNOS phosphorylation, whereas PP1, a potent Src tyrosine kinase inhibitor, had no effect (Figure 4A). Consistently, overexpression of Δp85, a dominant-negative mutant of the p85 regulatory subunit of PI3K, and DN-Akt, a dominant-negative mutant of Akt, inhibited RANKL-induced eNOS activation (Figure 4B-D). Taken together, these results indicate that RANKL stimulates the production of endothelial NO via a TRAF6-dependent PI3K/Akt signaling pathway acting on eNOS.

F4

NO is required for RANKL-induced migration and capillary-like network by ECs

RANKL induced the formation of extensive capillary-like networks of ECs cultured on 2-D Matrigel matrix, and this effect was almost completely inhibited by pretreatment with NMA (Figure 5A-B). Consistent with involvement of the eNOS activation pathway, RANKL-induced capillary-like network was blocked by Wortmannin, as well as by overexpression of DN-T6, but not of DN-T2 (Figure 5C-D). We next examined the role of NO in RANKL-induced EC migration. RANKL stimulated the chemotactic motility of HUVECs approximately 1.5-fold, and this effect was

F5

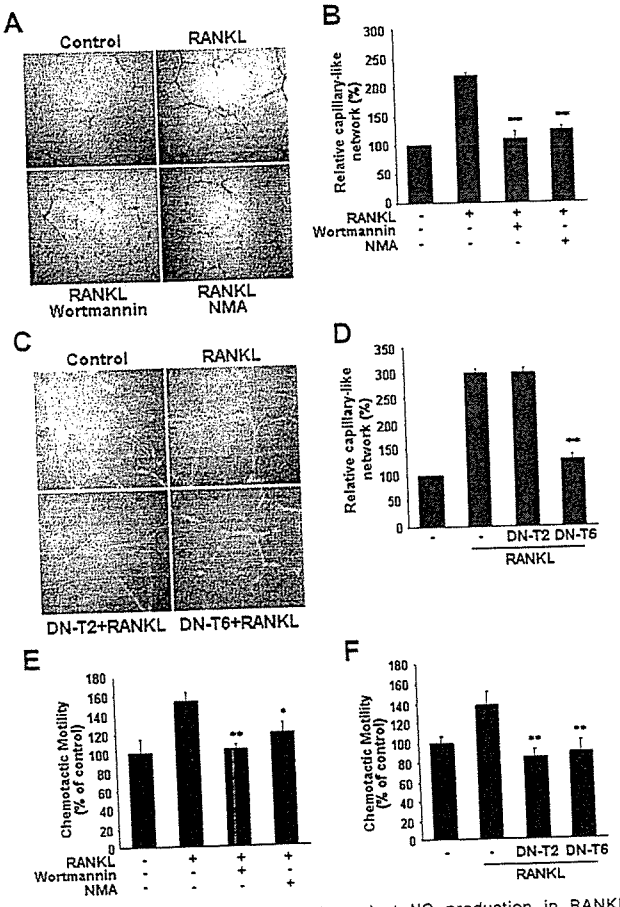

Figure 5. Involvement of PI3K/Akt-dependent NO production in RANKL-induced migration and capillary-like network by ECs. (A,E) HUVECs were preincubated for 30 minutes with or without 100 nM Wortmannin or 1 mM NMA prior to stimulation with RANKL (5 μg/mL). (C, F) HUVECs were stably transfected with DN-T2 and DN-T6 using retroviral system. (A,C) Cells were plated on Matrigel-coated plates at a density of 2×10^5 cells/well and incubated with 5 μg/mL RANKL. Microphotographs were taken after 20 hours (× 200). (B,D) Capillary-like networks were quantified with Image-Pro Plus software. (E-F) After 4 hours of incubation, chemotaxis was quantified with an optical microscopy. Three independent experiments were performed in duplicate. Data are means ± SDs: $^{*}P < .05$; $^{**}P < .01$ versus RANKL alone.

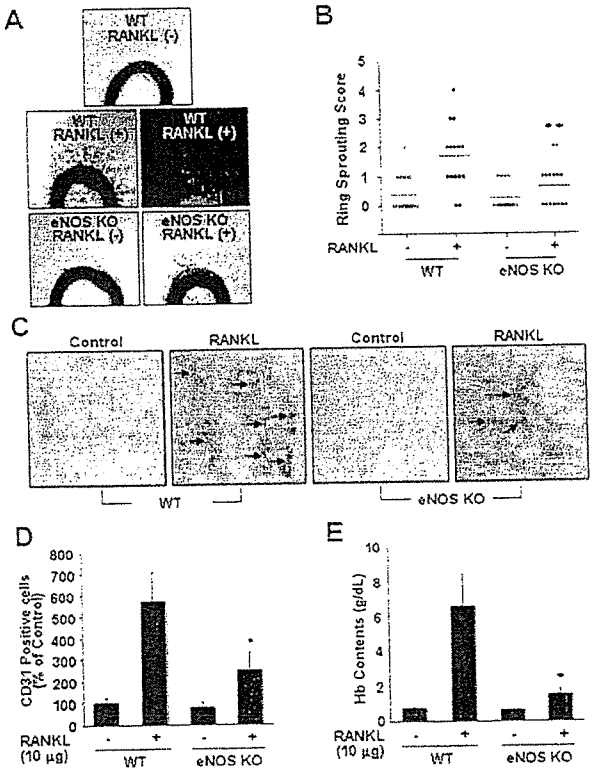

Figure 6. eNOS plays a critical role in RANKL-induced angiogenesis. (A) Aortic segments were harvested from WT and eNOS KO mice (n = 7 per group). Endothelial-cell sprouts forming branching cords from the margins of vessel segments taken from mice were photographed under a phase microscope. Staining of endothelial cells sprouted from RANKL-treated aorta with VWF (middle). (B) Sprouting scores were classified from 0 (least positive) to 5 (most positive). Data are means ± SEs. (C-E) WT and eNOS KO mice (n = 7 per group) were injected with 0.6 mL Matrigel containing RANKL (10 μg). After 7 days, the mice were killed and the Matrigel plugs were excised. (C) Plugs were stained for infiltrating endothelial cells using anti-CD31 antibody. Arrows indicate CD31$^+$ cells. (D) Quantitative assessment of CD31$^+$ endothelial cells. (E) Quantification of neovessel formation by measuring hemoglobin in the Matrigel. Data are means ± SDs: $^*P < .05$; $^{**}P < .01$ versus RANKL in WT.

abolished by Wortmannin and NMA, as well as by DN-T6 (Figure 5E-F). These results suggest that NO is required for the migration and differentiation of ECs in response to RANKL. In contrast to its lack of effect on EC capillary-like network, DN-T2 did inhibit the RANKL-induced increase in chemotactic motility of the HUVECs (Figure 5F), pointing to the involvement of NO-independent pathways activated by TRAF2 in RANKL-induced EC migration.

eNOS plays a critical role in RANKL-induced angiogenesis

To further assess the role of NO in RANKL-induced angiogenesis, we compared endothelial-cell sprouting in the aortic ring segments from eNOS KO and WT mice. RANKL caused a 3-fold increase in endothelial-cell sprouting in WT mice, but this effect was significantly abrogated in the aortic rings from eNOS KO mice (Figure 6A-B). Furthermore, RANKL-induced sprouting of endothelial cells in the rat aortic rings was stimulated by RANKL, and this angiogenic response was inhibited by simultaneous treatment with Wortmannin or NMA (Figure S3A-B). We further analyzed the role of endothelial cell–derived NO in RANKL-induced neovascularization in vivo. Matrigel containing RANKL was subcutaneously injected into WT and eNOS KO mice, and 7 days later the Matrigel plugs formed in the mice were excised and analyzed. There was nearly 70 g/L (7 g/dL) hemoglobin in the plugs of the WT mice, whereas those of the KO mice contained only about 18 g/L (1.8 g/dL) (Figure 6E). Plugs of the WT mice exhibited significantly higher densities of CD31$^+$ endothelial cells than those of KO mice (Figure 6C-D). Consistently, in a corneal micropocket assay, RANKL was less angiogenic in the eNOS KO mice than in the WT mice as measured by the numbers of neovessels (Figure S4A-B). AQ: 29

Discussion

The present results have revealed a novel action of RANKL, namely that of increasing vascular permeability in vitro and in vivo. Moreover RANKL can be added to the list of NO-dependent endothelial stimuli that promote both vascular leakage and angiogenesis. Our findings have implications for the role of RANKL in vascular physiology. Given its considerable adverse effects in adults, such as arterial calcification and inflammatory activation enhancing leukocyte adhesiveness,[3,29] our findings underline the possibility that RANKL is implicated in the development of vascular diseases.

Atherosclerosis has many characteristics in common with inflammatory disease characterized by infiltration of activated immune cells into the intima.[30] We have recently demonstrated that RANKL causes adhesion of leukocytes to ECs as a consequence of increased expression of cell adhesion molecules such as ICAM-1 and VCAM-1 in the ECs.[29] RANKL is produced by various cells, including vascular cells and activated immune cells close to blood vessels, and it exists in either a cell-bound or a secreted form.[3] Its expression, together with OPG, is also modulated by various factors such as the inflammatory cytokines, TNF-α and IL-1β.[3] Under some circumstances, the ratio of RANKL to OPG in the vascular area increases, and this change may activate endothelial cells, which are thought to be involved in promoting the early stage of atherosclerotic inflammation, which is characterized by increased endothelial permeability, up-regulation of adhesion molecules, and transendothelial migration of leukocytes.[31,32] Moreover, considering that angiogenesis and calcification are common features of advanced atherosclerotic lesions, the angiogenic and calcifying activities of RANKL may contribute to the development of atheromatous vessels.[33] Notably, this notion was supported by recent studies showing the enhanced expression of RANKL both in clinical and experimental atherosclerosis.[8] mRNA levels of RANKL were increased in T cells in patients with unstable angina accompanied by increased expression of RANK in monocytes.[8] In the apoE$^{-/-}$ mice, RANKL is significantly expressed within the atherosclerotic plaques, whereas no RANKL immunostaining was detected in the nonatherosclerotic vessel wall.[8] Furthermore, Bennett et al[9] have demonstrated that OPG inactivation results in larger and more calcified advanced lesions in the innominate arteries of older apoE$^{-/-}$ mice.

Vascular permeability is defined as the movement of fluids and molecules between blood vessels and the underlying tissues, and it is regulated by various inflammatory factors that break down intercellular endothelial junctions.[34] Although vascular leakage is not a prerequisite for blood vessel growth, increased vascular permeability often coincides with the early stage of angiogenesis and is also found in areas of diseased tissue in diabetic retinopathy, solid tumors, myocardial infarction, wounds, and chronic inflammation.[35] VEGF, originally isolated as a vascular permeability factor